Towards Automatic 3D Bone Marrow Segmentation

Chuong T. Nguyen[†], Joseph P. Havlicek[†], Jennifer Holter Chakrabarty[††], Quyen Duong[‡], and Sara K. Vesely[‡]
[†]*School of Electrical and Computer Engineering, University of Oklahoma*
[††]*College of Medicine, Hematology/Oncology, University of Oklahoma Health Sciences Center*
[‡]*Dept. of Biostatistics and Epidemiology, University of Oklahoma Health Sciences Center*

***Abstract*—Current noninvasive evaluation of bone marrow proliferation in leukemia treatment is limited to manually examining marrow tissue in multiple regions of interest (ROIs). The statistics extracted from these ROIs often fail to provide an accurate global characterization of the patient's marrow. We propose an automatic framework for segmenting spinal marrow compartments to characterize the bone marrow from full-body joint PET/CT scans acquired subsequent to bone marrow transplantation. We first apply a graph-cut algorithm to the CT volume to obtain a 3D full-body bone map. We then isolate the spinal column in a single sagittal plane where connected components labeling and iterative thresholding are used to segment the vertebral bodies. This fully automated approach achieves an average accuracy of 91.7% and a worst case accuracy of 80.4% in testing on 51 scans of 17 patients. Finally, we outline a method for rejecting the cortical bone in transverse planes that can be combined with the sagittally segmented vertebral bodies to obtain a 3D map of the vertebral body medullary cavities for the entire spine.**

***Keywords*-3D bone segmentation, bone marrow extraction, SUV, PET/CT**

I. Introduction

Recent studies show that ^{18}F-fluoro-L-deoxythymidine (FLT) can be used in conjunction with PET/CT imaging to enable non-invasive diagnosis and monitoring of patient recovery subsequent to bone marrow transplantation [1]–[5]. In clinical practice, bone marrow proliferation measurements are extracted by analyzing the PET/CT scans with commercial medical software packages that measure growth statistics from multiple ROIs to evaluate the patient's condition [4], [5]. However, manual designation of large numbers of ROIs is both time and labor intensive, whereas a sparse collection of ROIs may fail to sufficiently characterize the entire marrow compartment. In addition, the manual designation of consistent, identical ROIs in scans of a single patient acquired over time is nontrivial. These considerations strongly motivate the need for an automated technique capable of segmenting and spatiotemporally registering the medullary cavity.

3D semi-automatic or automatic bone segmentation algorithms have been widely reported in the literature. Krčah et al. [6] used graph-cut to segment bone tissue into multiple classes. Kang et al. [7] used a hierarchical approach combining adaptive thresholding and region growing to perform 3D bone segmentation. Mastmeyer et al. [8] also used a hierarchical scheme where region growing was followed by segmentation of the vertebrae via detection of the disks between them. Yao et al. [9] and Klinder et al. [10] proposed algorithms to locate the spinal column by detecting the spinal cord. Huang et al. [11] used training with Adaboost to construct vertebrae detectors. Glocker et al. [12] used a supervised classification forest to detect vertebrae shapes and label them. Most of these methods are limited to the segmentation of an entire bone or bone structure as a unit and none of them can directly differentiate between cancellous and cortical bone tissue. Thus they cannot be readily generalized to extract the medullary cavities inside the vertebral bodies of the spinal column, which is a challenging task because the vertebrae must be isolated from the larger bone structure and the boundary between the cortex and medullary cavities must be robustly detected.

In this paper, we introduce a new, fully automatic framework for segmenting the marrow compartments of the human spinal column from CT data and for measuring standard biomarker uptake value (SUV) from joint PET data. We use a graph-cut segmentation [13] to obtain an initial coarse 3D map of the full-body bone volume. We then refine this segmented volume to extract the vertebral bodies. Local gradient drop-off detection and smooth curve fitting are then applied to reject the cortex, retaining only the medullary cavities. Once the medullary cavities are isolated in the CT data, measurement of the SUV is relatively straightforward and consists primarily of registering the PET and CT voxels. To the best of our knowledge, this is the first automatic 3D bone marrow segmentation method specifically targeted to diagnosing and monitoring the recovery process of bone marrow transplantation patients. The closest existing work in the literature is that by Sambucetti, et al. [14], who also measured bone marrow SUV. However, they performed a 2D active contour segmentation on a per-slice basis to construct the 3D bone volume and their method requires manual supervision by a human expert.

II. Segmentation Framework Overview

An overview of the proposed method is given in Fig. 1. We use a 3D bilateral filter to smooth certain artifacts that may be present in the CT volume acquired from patients who have undergone marrow ablation. The initial 3D bone volume is then obtained by applying the 3D graph cut algorithm [13]. We next refine the bone volume to retain only the vertebral bodies of the spinal column. Finally, the cortex of each vertebra is rejected to obtain an accurate map of the medullary cavities.

A. Volume Smoothing

Our main interest is in developing an automatic method for segmenting the marrow compartment to facilitate efficient and accurate evaluation of bone marrow proliferation in leukemia patients whose treatment includes allogeneic bone marrow transplantation. In such patients, bone marrow ablation with total body irradiation and chemotherapy is typically performed prior to the transplant in order to eradicate diseased tissue. As mentioned in the preceding

This work was supported in part by grants from the Oklahoma Clinical and Translational Science Institute, the University of Oklahoma Center for Biomedical Engineering, and the University of Oklahoma Stephenson Cancer Center.

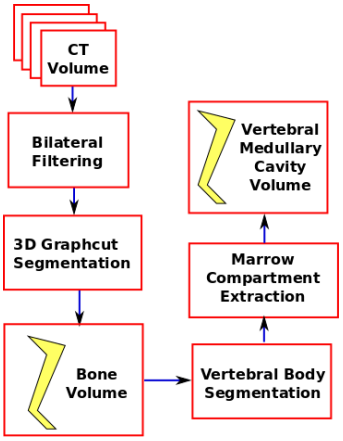

Figure 1. Block diagram of spinal column segmentation method.

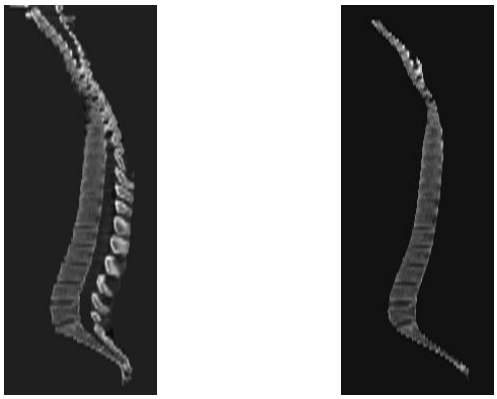

(a) Original sagittal slice. (b) Vertebral body filtering.

Figure 2. The full-body bone volume obtained from graph-cut segmentation (a) is filtered to reject the vertebral arches in (b).

paragraph, the CT images acquired from these patients may contain undesirable non-smooth artifacts, particularly near the boundaries of the cortical bone tissue. We observed these artifacts most commonly in the CT volumes acquired one day prior to and five or nine days subsequent to transplantation.

Therefore, prior to segmentation we apply a 3D bilateral filter [15], [16] to remove any artifacts that may have been induced by the conditioning regimen. The bilateral filter is a smoother that performs neighborhood averaging using weights given by the product of a spatial distance kernel and an intensity (range) kernel that are normally both Gaussian; it can smooth spurious noise and artifacts while retaining the strong edges of the cortical bone tissue. For parameter tuning, we set the spatial bandwidth to $\sigma_s = 2$, the range bandwidth to $\sigma_r = 5$, the spatial sampling factor to $\mathrm{S}_s = 5$, and the range sampling factor to $\mathrm{S}_r = 15$.

B. Graph-Cut Segmentation

In general, bone tissue tends to exhibit higher CT intensities relative to non-bone material such as water, air, and muscle. Closely following the implementation described in [17], we use the graph-cut segmentation algorithm [6], [13] which optimizes a global energy function consisting of a per-pixel component that penalizes misclassified voxels and a boundary component that enforces spatial coherence of the segmented objects.

Let $\mathcal{N}$ be a system of symmetric 7-voxel 3D cross-shaped neighborhoods on the 3D CT volume and let I_p be the intensity of bilateral filtered CT voxel p in Hounsfield units. Each voxel is assigned a label A_p according to

$$A_p = \begin{cases} 1, & \text{if voxel } p \text{ classified as "bone,"} \\ 0, & \text{if voxel } p \text{ classified as "not bone."} \end{cases} \quad (1)$$

As in [6], the labels A_p are assigned by minimizing the energy function

$$\mathcal{E} = \sum_p R_p(A_p) + \lambda \sum_{p,q \in \mathcal{N}} \delta(A_p, A_q) B(p,q), \quad (2)$$

where $\lambda = 0.03$, $\delta(\cdot)$ is the Kronecker delta, and

$$R_p = \begin{cases} 1, & A_p = 1 \text{ and } I_p < T_l, \\ 1, & A_p = 0 \text{ and } I_p > T_h, \\ 0, & \text{otherwise.} \end{cases} \quad (3)$$

The high and low thresholds T_h and T_l are set to -50 and 200 Hounsfield units, respectively, and were determined through empirical analysis of the bilateral filtered CT volume data. Unlike [6], we use a simplified boundary penalty given by $B(p,q) = \exp(-|I_p - I_q|/\sigma)$ with $\sigma = 10$.

C. Vertebral Body Segmentation

Let $p = (i,j,k)$ denote the 3D coordinate of a CT voxel, where i,j,k are the coronal, sagittal, and transverse slice indices. The full-body bone volume $V(i,j,k) = A_p$ obtained from the segmentation in Section II-B is a 3D binary mask that is one at voxels classified as bone by (1)-(3). Thus, V contains not only the spinal column, but also other bone structures such as ribs, sternum, femur, and skull. A common approach for extracting the spinal column is to detect the spinal cord and retain only the bone voxels lying ventral to it [9], [10]. Here, we propose an alternate approach to extract only the vertebral bodies by iterative thresholding.

We estimate the slice index j^* of the mid-sagittal plane by

$$j^* = \arg\max_j \sum_{i,k} V(i,j,k), \quad (4)$$

which selects the sagittal slice containing the most bone voxels. An initial mask $\tilde{\mathcal{M}}(i,k) = V(i,j^*,k)$ then provides a coarse approximate 2D map of the spinal column. However, $\tilde{\mathcal{M}}(i,k)$ will generally contain disconnected blobs due to missed detections, particularly in patients with some degree of scoliosis, and may also contain false alarms arising from bones that are not part of the spinal column. Therefore, we expand the search window to adjacent parasaggital slices and compute

$$\mathcal{C}(i,k) = \sum_{j=j^*-L}^{j^*+L} V(i,j,k), \quad (5)$$

where $L = 10$ is typical and was used for all results reported in this paper. We then define a refined 2D vertebral body mask

$$\mathcal{M}_T(i,k) = \begin{cases} 1, & \mathcal{C}(i,k) > T, \\ 0, & \text{otherwise,} \end{cases} \quad (6)$$

parameterized by a threshold T. For $T = 0$, the mask $\mathcal{M}_0(i,k)$ will overestimate the volume of the vertebral bodies and will

Table I
SEGMENTATION DETECTION RATE PERCENTAGE OF THE PROPOSED METHOD VERSUS GROUND TRUTH DATA FOR FINAL 2D MASK $\mathcal{M}$

Patient	D_1 (%)	D_2 (%)	D_3 (%)
1	91.3543	91.3242	96.7351
2	87.7176	94.3374	87.8991
3	92.6192	95.0623	97.2303
4	95.6184	85.8534	95.9717
5	88.9908	92.0755	93.0146
6	89.4424	89.9807	93.1200
7	92.4500	90.3509	85.0135
8	90.6667	91.9328	87.0615
9	88.0000	90.7464	97.2117
10	95.2839	93.5194	92.9558
11	87.9641	90.6900	92.0195
12	89.1392	94.7438	92.1324
13	96.4789	85.7780	91.6041
14	97.7213	96.6728	96.1581
15	94.3219	92.4466	91.8040
16	86.1133	88.9731	80.4086
17	90.8038	91.8389	93.6111

contain many false alarms. To obtain the final 2D vertebral body mask $\mathcal{M}(i,k)$, we initialize the threshold to zero and iteratively increment it to the smallest value for which only a single 8-connected component remains in $\mathcal{M}_T(i,k)$. A final application of connected components labeling with minor region removal to the complement of $\mathcal{M}(i,k)$ then removes any remaining holes.

An example vertebral body filtering result appears in Fig. 2. In Fig. 2(a), a graph-cut segmented sagittal slice includes the vertebral bodies and extra components such as the spinal canal, lamina and spinous process. The proposed algorithm retains the vertebral bodies in Fig. 2(b) while rejecting the unwanted components.

As a baseline performance evaluation, we compute the correct detection rate D of the final 2D vertebral body mask $\mathcal{M}(i,k)$ relative to manually labeled ground truth $G(i,k)$ according to

$$D = 100 \times \frac{|\mathcal{M} \cap G|}{|G|}, \tag{7}$$

where $|\cdot|$ denotes the sum of bone voxels. Intuitively, D measures the percentage overlap between the automatically delivered mask $\mathcal{M}(i,k)$ and the ground truth bone mask designated by an expert physician. A perfect segmentation result is 100%. The experimental results obtained with our proposed method are given in Table I. Each row shows correct detection rates D_i, $i \in \{1,2,3\}$, corresponding to three scans of the same patient imaged on three different days. Even for the same patient, we expect variations in measured results because the subject may move or lay at different positions and angles or may have experienced actual morphological changes. For these 17 patients, all of whom received myeloablative hematopoietic stem cell transplantation, our method achieves a worst case performance of 80.4% while the average is $> 91\%$.

To obtain the 3D vertebral body volume, we superimpose the final 2D mask $\mathcal{M}(i,k)$ on the j^* sagittal slice of the CT volume. The mask intersects each transverse CT slice in a line segment where $\mathcal{M}(i,k) = 1$. On a slice-by-slice basis, we rotate this line segment about a longitudinal axis passing through its midpoint to sweep out a circle in the transverse plane that selects CT voxels for inclusion in the segmented 3D vertebral body volume.

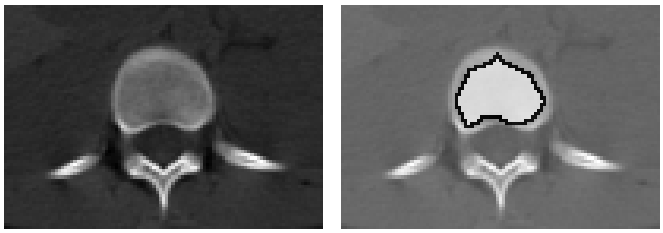

(a) Original CT. (b) Marrow compartment.

Figure 3. Bone marrow extraction from a CT slice in a transverse plane. (a) Original CT slice with vertebra. (b) Bone marrow compartment is shown in the white masked area with black surrounding contour.

III. EXTRACTION OF SPINAL MARROW COMPARTMENT

The filtering algorithm in Section II-C results in a refined spinal volume that contains only the vertebral bodies. However, each of these vertebral bodies contains both cortical and cancellous bone tissue. The cancellous bone is located inside the cortical bone and usually exhibits lower intensity. Therefore, the cancellous bone regions that are of interest for assessing proliferation can be extracted by detecting the sharp transitions of voxel intensity between the cortical and cancellous tissue.

We currently use an extremely simple strategy to detect the transitions; development of a more sophisticated approach is an important component of our ongoing work. We process the CT transverse slices sequentially. For each slice that intersects the 3D vertebral body volume segmented in Section II-C, we mark the spatial centroid of the vertebral body. We then construct lines ℓ_c and ℓ_s through the centroid and parallel to the coronal and sagittal axes, respectively. For each CT voxel on the perimeter of the vertebral body, we traverse a perpendicular connecting the voxel to ℓ_c. At each voxel along this path, we compute the derivative of CT intensity in the direction of traversal. The largest magnitude transition from positive to negative derivative is marked as a boundary point of the marrow compartment. This procedure is then repeated for a perpendicular connecting each perimeter voxel to ℓ_s. To segment the marrow compartment, we construct a closed curve through the set of detected boundary points and use interpolation for any rows and columns where no significant transition from positive to negative derivative was observed. Voxels interior to this curve are labeled as part of the marrow compartment. The procedure is illustrated in Fig. 3, where the original transverse CT slice is shown in Fig. 3(a). In Fig. 3(b), the detected marrow compartment boundary is shown as a black contour and the medullary cavity is shown in white. The final 3D map of the entire spinal marrow compartment is obtained by concatenating the cavities detected in each transverse slice.

IV. DISCUSSION AND CONCLUSION

We introduced an automatic 3D bone marrow segmentation framework that consists of three main components including a coarse full-body graph-cut segmentation, spinal column vertebral body segmentation, and cancellous region extraction. We demonstrated the effectiveness of the proposed method on joint PET/CT images of 17 patients who underwent bone marrow transplantation. Each patient was imaged three times during the treatment regimen,

typically one day before, one week after, and one month after transplant. In each case, we used the final 3D map of the full spinal marrow compartment obtained from the CT data as described in Section III to measure FLT SUV from the PET data by registering the CT and PET volumes via a standard mutual information model and affine deformation [18].

Once the CT and PET volumes are registered, it becomes relatively straightforward to calculate FLT SUV over the intersection of the PET volume and spinal marrow compartment map, the only significant challenge being the need for interpolation at the boundaries of the segmented marrow compartment to account for the physical size difference between voxels in the two modalities. Statistics of the FLT SUV including the mean, median, max, and variance provide important cues for evaluating bone marrow proliferation in patients who have undergone myeloablative hematopoietic stem cell transplantation. An emerging hypothesis is that shape features of the 3D SUV distribution such as curvature, smoothness, and regularity may also be important. Whereas FLT SUV measurement is limited to a relatively small number of manually designated ROIs in current clinical practice, the automatic segmentation framework presented here could potentially enable comprehensive evaluation of the entire marrow compartment.

V. Acknowledgement

The authors are grateful to Dr. Kirsten M. Williams, M.D., of the National Cancer Institute (NCI), NIH, for consenting and conducting the clinical trial, including caring for patients and performing evaluation and analysis of the clinical and experimental data, to Dr. Ronald E. Gress, M.D., Chief, Experimental Transplantation and Immunology Branch, NCI/NIH, for sponsoring the clinical trial, to Dr. M. Liza Lindenberg, M.D., of the Molecular Imaging Program, NCI/NIH, for supervising the image capture, collating images, and reviewing and editing the manuscript, and to Dr. Peter L. Choyke, M.D., Director, Molecular Imaging Program, NCI/NIH, for sponsoring the clinical trial and providing imaging oversight. The work reported here would not have been possible without their valuable contributions.

References

[1] A. Shields, J. Grierson, B. Dohmen, H.-J. Machulla, J. Stayanoff, J. Lawhorn-Crews, J. Obradovich, O. Muzik, and T. Mangner, "Imaging proliferation *in vivo* with [F-18]FLT and positron emission tomography," *Nature Med.*, vol. 4, pp. 1334–1336, 1998.

[2] D. Cobben, P. Elsinga, H. Hoekstra, A. Suurmeijer, W. Vaalburg, B. Maas, P. Jager, and H. Groen, "Is 18F-3'-fluoro-3'-deoxy-L-thymadine useful for the staging and restaging of non-small cell lung cancer?" *J. Nucl. Med.*, vol. 45, no. 10, pp. 1677–1682, 2004.

[3] A. Buck, M. Bommer, M. Juweid, G. Glatting, S. Stilgenbauer, F. Mottaghy, M. Schulz, T. Kull, D. Bunjes, P. Möller, H. Döhner, and S. Reske, "First demonstration of leukemia imaging with the proliferation marker 18F-fluorodeoxythymidine," *J. Nucl. Med.*, vol. 49, no. 11, pp. 1756–1762, 2008.

[4] A. Agool, R. Start, P. Kluin, J. de Wolf, R. Dierckx, and E. Vellenga, "F-18 FLT PET: a noninvasive diagnostic tool for visualization of the bone marrow compartment in patients with aplastic anemia: A pilot study," *Clin. Nucl. Med.*, vol. 36, no. 4, pp. 286–289, 2011.

[5] J. Hayman, J. Callahan, A. Herschtal, S. Everitt, D. Binns, R. Hicks, and M. Mac Manus, "Distribution of proliferating bone marrow in adult cancer patients determined using FLT-PET imaging," *Int'l. J. Radiation Oncology Biol. Phys.*, vol. 79, no. 3, pp. 847–852, 2011.

[6] M. Krčah, G. Székely, and R. Blanc, "Fully automatic and fast segmentation of the femur bone from 3D-CT images with no shape prior," in *Proc. IEEE Int'l. Symp. Biomed. Imag.*, Mar. 2011, pp. 2087–2090.

[7] Y. Kang, K. Engelke, and W. Kalender, "A new accurate and precise 3-D segmentation method for skeletal structures in volumetric CT data," *IEEE Trans. Med. Imag.*, vol. 22, no. 5, pp. 586–598, May 2003.

[8] A. Mastmeyer, K. Engelke, C. Fuchs, and W. Kalender, "A hierarchical 3D segmentation method and the definition of vertebral body coordinate systems for QCT of the lumbar spine," *Med. Image Anal.*, vol. 10, no. 4, pp. 560–577, 2006.

[9] J. Yao, S. O'Connor, and R. Summers, "Automated spinal column extraction and partitioning," in *Proc. IEEE Int'l Symp. Biomed. Imag.*, Apr. 2006, pp. 390–393.

[10] T. Klinder, J. Ostermann, M. Ehm, A. Franz, R. Kneser, and C. Lorenz, "Automated model-based vertebra detection, identification, and segmentation in CT images," *Med. Image Anal.*, vol. 13, no. 3, pp. 471–482, 2009.

[11] S.-H. Huang, Y.-H. Chu, S.-H. Lai, and C. Novak, "Learning-based vertebra detection and iterative normalized-cut segmentation for spinal MRI," *IEEE Trans. Med. Imag.*, vol. 28, no. 10, pp. 1595–1605, Oct. 2009.

[12] B. Glocker, D. Zikic, E. Konukoglu, D. Haynor, and A. Criminisi, "Vertebrae localization in pathological spine CT via dense classification from sparse annotations," in *Proc. Int'l. Conf. Med. Image Comput. Comput. Assist. Interv.*, 2013, pp. 262–270.

[13] Y. Boykov and V. Kolmogorov, "An experimental comparison of min-cut/max-flow algorithms for energy minimization in vision," *IEEE Trans. Pattern Anal. Mach. Intell.*, vol. 26, no. 9, pp. 1124–1137, Sep. 2004.

[14] G. Sambuceti, M. Brignone, C. Marini, M. Massollo, F. Fiz, S. Morbelli, A. Buschiazzo, C. Campi, R. Piva, A. Massone, M. Piana, and F. Frassoni, "Estimating the whole bone-marrow asset in humans by a computational approach to integrated PET/CT imaging," *Eur. J. Nucl. Med. Mol. Imaging*, vol. 39, no. 8, pp. 1326–1338, 2012.

[15] C. Tomasi and R. Manduchi, "Bilateral filtering for gray and color images," in *Proc. IEEE Int'l. Conf. Comput. Vision*, Bombay, India, Jan. 4-7, 1998, pp. 839–846.

[16] S. Paris and F. Durand, "A fast approximation of the bilateral filter using a signal processing approach," *Int. J. Comput. Vis.*, vol. 81, no. 1, pp. 24–52, 2009.

[17] S. Bagon, "Matlab wrapper for graph cuts," December 2006, http://www.wisdom.weizmann.ac.il/~bagon.

[18] F. Maes, D. Vandermeulen, and P. Suetens, "Medical image registration using mutual information," *Proc. IEEE*, vol. 91, no. 10, pp. 1699–1722, Oct. 2003.